Polymer Chemistry

Visible light-Induced surface grafting polymerization of perfluoropolyether brushes as marine low fouling materials

Journal:	*Polymer Chemistry*
Manuscript ID	PY-ART-02-2023-000126.R1
Article Type:	Paper
Date Submitted by the Author:	16-Mar-2023
Complete List of Authors:	Manderfeld, Emily; Ruhr-Universität Bochum, Analytical Chemistry - Biointerfaces Balasubramaniam, Ajitha; Ruhr-Universität Bochum, Analytical Chemistry - Biointerfaces Özcan, Onur ; Ruhr-Universität Bochum, Analytical Chemistry - Biointerfaces Anderson, Charlotte ; Newcastle University, School of Natural and Environmental Sciences Finlay, John; Newcastle University, School of Natural and Environmental Sciences Clare, Anthony; Newcastle University, School of Natural and Environmental Sciences Hunsucker, Kelli ; Florida Institute of Technology, Center for Corrosion and Biofouling Control Swain, Geoffrey; Florida Institute of Technology, Center for Corrosion and Biofouling Control Rosenhahn, Axel; Ruhr-Universität Bochum, Analytical Chemistry - Biointerfaces

Visible light-Induced surface grafting polymerization of perfluoropolyether brushes as marine low fouling materials

Emily Manderfeld[1], Ajitha Balasubramaniam[1], Onur Özcan[1], Charlotte Anderson[2], John A. Finlay[2], Anthony S. Clare[2], Kelli Hunsucker[3], Geoffrey W. Swain[3], and Axel Rosenhahn[1*]

[1]Analytical Chemistry - Biointerfaces, Ruhr University Bochum, 44780 Bochum, Germany
[2]School of Natural and Environmental Sciences, Newcastle University, Newcastle upon Tyne NE1 7RU, United Kingdom
[3]Center for Corrosion and Biofouling Control, Florida Institute of Technology, Melbourne, Florida 32901, United States

* corresponding author: axel.rosenhahn@rub.de

Abstract

Perfluoropolyether dimethacrylate (PFPE-DMA) was polymerized onto surfaces via visible light-induced surface grafting polymerization. Surfaces were prepared by depositing an octadecyltrichlorosilane-monolayer on the substrates, followed by the covalent coupling of the photoinitiator isopropylthioxanthone. Subsequently, perfluoropolyethers were polymerized from the surface by the controlled use of visible light-induced surface grafting polymerization. This approach was used to obtain surfaces terminated by low surface energy PFPE-DMA brushes with different chain lengths. Coating thickness and wetting were characterized by spectroscopic ellipsometry and contact angle goniometry. Different coating thicknesses were tested for their antifouling properties against three different proteins (lysozyme, fibrinogen, bovine serum albumin). In addition, the coatings were subjected to biological evaluation against the attachment of the diatom *Navicula perminuta* under dynamic conditions, settlement of *Ulva linza* zoospores, and in dynamic short-term field immersion experiments. PFPE-DMA with the highest chain length showed the strongest fouling reduction, which indicates that a certain chain mobility supports fouling resistance which could be explained by an improved lubricity of the interface.

1. Introduction

The colonization and growth of marine organisms on submerged surfaces is known as marine biofouling. (1) Overgrown material negatively affects maritime activities, including shipping and leisure vessels, aquaculture systems, and heat exchangers. Marine biofouling has not only environmental but also economical penalties. Deposition and growth of biofilms cause an increase in fuel consumption due to an increased drag on the moving ships(2), leading to higher costs and an additional demand for cleaning. (3) Furthermore 30% of the smog-forming nitrogen oxide gases are emitted from ships, as well as 3% of all anthropogenic CO_2. (2)

Most modern coatings use combinations of biocides to reduce fouling on ships' hulls. (4) While these coatings are very effective in preventing biofouling, released biocides may accumulate in harbors, dry docks, and along shipping routes with adverse consequences for non-target organisms. (5,6) As non-toxic, biocide-free alternatives, fouling-release coatings (FRC), to which organisms can only adhere weakly and which have the ability to self-clean at sufficient cruising speeds, have been developed. (1) Silicone elastomers such as polydimethylsiloxane (PDMS) are the most frequently used FRC. (7,8) Their low cost, low critical surface energy, chemical and thermal stability, as well as smooth surface structure and low elastic modulus make them ideal candidates for environmentally benign coating technologies. (9,10) The hydrophobicity of PDMS is, however, not per-se anti-adhesive and especially under static conditions cells can adhere. (9) It has long been recognized that the addition of oils into silicone coatings enhances their FR performance. (11) Besides silicones and silicone oils, perfluoroether compounds were also discovered to possess interesting low-fouling properties. (12–14) Perfluoropolyether (PFPE) lubricants enhance the performance of silicones and are used in FRCs. (15) PFPE lubricants exhibit a low surface energy (12-20 $mN \cdot m^{-1}$) and a low glass transition temperature (120 °C to -70°C), as well as a good chemical and thermal stability. (14) They feature non-sticking characteristics due to their low critical surface energy. The most commonly used fluorinated polymers are PFPE and fluorinated (meth)acrylates, both of which have low toxicity with a backbone flexibility similar to that of PDMS. (8) Non-crosslinked PFPE chains are frequently applied as lubricants in industry and a variety of viscosities is available for different applications. If such oils are applied to hydrophobic, porous surfaces, so called lubricant infused interfaces can be prepared with excellent low-fouling properties, which are termed SLIPS (slippery liquid infused surfaces). (16,17)

For oil infused coatings, the viscosity of the oil and its interaction with the matrix determine the

physicochemical properties of the coating such as contact angle, sliding angle (SA), and sliding velocity (SV) of a water droplet at the interface of the coatings. (18) Porous polymer films infused with silicone oils of varying viscosities, from 2 to 100 cst, showed similar contact angles and an increase in SA with increasing viscosity. Furthermore, a decrease in SV was reported with increasing viscosity of the oils. Several other studies(19,20) reported the increase in SA and decrease in SV with increasing silicone oil viscosity.

Not only lubricants, but also PFPE-based materials show very good antifouling properties. The suppression of non-specific adsorption of proteins by PFPE methacrylates is as good as on the corresponding PEG polymers. (21) Fluorogel elastomers composed of photocured perfluorinated acrylates and incorporated fluorinated lubricants also showed excellent antifouling behaviors against proteins. (22) In a different study, photochemically cross-linked PFPE based elastomers showed lower settlement of zoospores of *Ulva linza* and removal of sporelings comparable to that of a PDMS elastomers. (23) PFPE-based cross-linkable random terpolymers, which were obtained through the combination of a methacryldiamide-PFPE macromonomer, an alkyl (meth)acrylate, and a glycidylmethacrylate allowed a higher degree of cross-linking to be achieved and consequently a reduction in the mobility of the polymer chains. (14)

As both, the crosslinking of polymers and the viscosity of added oils have an influence on the material properties, this work aims on understanding if the chain length of PFPE brushes changes its fouling-release properties. Polymer brushes provide control over both the grafting density and the length of polymers on surfaces. Direct polymerization from initiating sites is known as surface-initiated polymerization. The high degree of synthetic control can be used to tailor the surface properties to specific needs and applications. (24–26) As the brushes are inherently ‘crosslinked’ at the surface, shorter chains will have less structural flexibility, while longer chains are able to move more freely. This leads to a lower surface friction as shown by a set of self-assembled monolayers terminated by different chain length. (27) It was shown, that the chain length of aliphatic self-assembled monolayers has an influence on the fouling release properties on the surfaces, as longer chains are associated with a higher lubricity of the chains. (28) The friction coefficients also depend on the packing density, as lower densities lead to lower film thicknesses and consequently to higher friction coefficients. (29)

A facile way to prepare polymer brushes is by grafting-from polymerization. For this method, initiators are immobilized on surfaces and subsequently a controlled polymerization, starting from the initiator furthest away from the surface, is induced. The most popular methods are atom transfer radical polymerization (ATRP) and reversible-addition-fragmentation chain-transfer polymerization (RAFT) polymerization. We recently published a method for visible light-induced controlled surface grafting polymerization as a versatile platform for surface modification. (30) The method starts with the deposition of a thin layer of octadecyl trichlorosilane (OTS) and subsequent photoimmobilization of isopropylthioxanthone (ITX). Irradiation with visible light (385 nm) led to the activation of the dormant ITX groups and initiated the surface grafting polymerization reaction. Using visible light (385 nm) this method has the advantage that a variety of monomers can be used and that the polymerization will only

occur while the illumination is switched on.

In this work we evaluate the importance of the PFPE chain mobility and determine which synthesis conditions allow the tethered chains to reach a chain length at which antifouling or fouling-release activity is created. Therefore, perfluoropolyetherdimethacrylat (PFPE-DMA) was polymerized by an ITX mediated grafting-from polymerization onto a substrate. PFPE-DMA brushes with defined thickness were grown on the surface by changing the illumination time. The coatings were analyzed by contact angle goniometry, ellipsometry and challenged against the adhesion of proteins, different marine fouling organisms, and in short-term field exposures.

2. Materials and Methods

Purchased chemicals and materials Acetone p.a. (Sigma-Aldrich, ≥ 99.5 %), chloroform (Fischer Chemicals, ≥ 99.8 %), cyclohexane (Fisher Chemicals, ≥ 99.99 %), ethanol (Roth, ≥ 99.8 %, p.a.) and toluene (Fisher Chemicals, ≥ 99.98 %) were used as solvents as received. 2-Isopropylthioxanthone (ITX, TCI ≥ 98.0 %) was bought from TCO, recrystallized once from ethanol, and stored at -20 °C. Fluorolink MD 700 (PFPE-DMA, Acota ≥ 99.8 %) was used as received. Distilled water was purified by a Milli-Q-Plus system (Siemens). Silicon wafers (<100> orientation, 100 mm diameter, 525 µm thickness, prime quality) were obtained from Siegert Wafer and stored under an argon atmosphere. NexterionB (clean room cleaned) glass slides were obtained from Schott (Jena, Germany).

Light sources for photochemistry For the coupling of ITX, a 254 nm UV light source (Osram Sylvania G8W) was used. A LED system with a 385 nm Nichia NVSU233A-D1 U385 UV LED (Nichia Corporation. Cat.No.151224; Tokushima, Japan, 2016.1000 mA, 3.65 V, 385 nm peak wavelength, 11 nm spectrum half width, 1400 mW radiant flux, 60° viewing angle, relative radiant intensity of 1 within ± 10° radiation angle and ≥ 0.9 within ± 40° and an irradiation intensity of 72 mW/cm^2) was used for the photo polymerization. Cooling for the high-power UV LED was achieved with an EK Water Blocks EK-Supremacy MX processor water cooler using Arctic Cooling Silver V heat conduction paste.

Preparation of OTS-monolayers The preparation of the OTS monolayers was performed as described in previously published protocols.(30) In brief, silicon wafers were cleaned and activated in an oxygen plasma (GaLa miniFlecto MFC plasma cleaner, argon oxygen plasma, 0.4 mbar, 80 W, 22 kHz, 3 min). The activated silicon substrates were used instantaneously. For the biological assays, Nexterion glass slides were used and activated by the same method as the silicon wafers. The plasma activated substrates were inserted into a silanization reactor(30) and a 0.5 mM solution of octadecyltrichlorosilane (≥ 90 %) (OTS,

Sigma-Aldrich) in a cyclohexane/chloroform solvent mixture (v/v, 75:25) was added though a dropping funnel, under a nitrogen atmosphere, and allowed to react for 30 min during ultrasonication (150 W) at reduced temperature (10-15°C). After the silanization, the samples were removed from the silane solution and sonicated for 3 min in a mixture of cyclohexane and toluene (75:25). Samples were retrieved and residual solvent was quickly removed in a nitrogen stream.

Photografting of ITX semipinacol ''dormant'' groups on OTS films by UV irradiation Photografting of ITXSP on OTS was performed as described in previously published protocols.(30) In brief, a 0.5 M solution of 2-Isopropylthioxanthone (98.0 %) (TCI, recrystallized from ethanol) in acetone was placed in a Schlenk tube and degassed three times using the freeze-pump-thaw method. Afterwards, the OTS coated substrates were placed into a Schlenk tube and exposed to 254 nm UV light for 3 min. After irradiation, the samples were rinsed with acetone and immersed in an acetone bath for 30 min to remove non-covalently attached ITX.

Visible light-induced grafting polymerization of PFPE-DMA The grafting-from photopolymerization followed previously established methods.(30) The polymerization was carried out in solutions of 0.1 wt%, 0.25 wt% and 0.5 wt% of PFPE-DMA in acetone. The solutions were degassed for 10 min with N2 and treated with the freeze-pump-thaw method three times to remove oxygen which could inhibit the polymerization. To prepare surfaces for the stability tests and the biological assays, concentrations of 0.5 wt% were chosen. The OTS-ITXSP modified surfaces were inserted into a Schlenk tube and immersed in the monomer solution. The polymerization was started by LED illumination with a wavelength of 385 nm at an LED-sample distance of around 3 cm for the desired time. After the polymerization reaction was completed, samples were retrieved, placed in degassed acetone for 24 h to leach out uncoupled monomers and dried in a stream of nitrogen. ITXSP groups were removed by immersion of the surfaces into acetone, which had been purged for 15 min with oxygen prior to immersion. The samples were irradiated for 10 min by a 385 nm LED to activate and quench the dormant ITXSP groups. Subsequently, the samples were immersed in a degassed acetone bath and leached for a further 24 h. The polymer brushes thus obtained were labeled pPFPE_x with x being the average height of the brushes in nm.

Contact angle goniometry The static water contact angles (CA) were measured using a custom-built goniometer. After deposition of the droplets (MiliQ water) on the samples, their shapes were recorded via a CCD camera and the contact angle was determined at the solid/liquid/gas intersection. The presented values were obtained from three measurements on each of at least three replicates per brush length. The error bars represent the standard error of the mean (SE).

Spectroscopic ellipsometry To determine the thickness of the pPFPE brushes and of the adsorbed protein layers, spectroscopic ellipsometry measurements were performed with a M2000 (JA Woollam Co., Inc.) operating in a wavelength range between 280 and 800 nm. All samples were measured before assembly and modeled as a B-spline. The polymer film was modeled as a transparent organic adlayer with a wavelength dependent refractive index described by a Cauchy model (A = 1.45, B = 0.01, C = 0). A

xenon lamp with a polychromatic spectrum was used as the light source. On each sample three measurements were performed at different positions and the reported values are the average of these three measurements. The error bars represent the standard deviation.

Infrared spectroscopy (ATR-FTIR) ATR-FTIR (VariGATR, Harrick, USA) spectra were obtained with a Bruker Tensor 27 spectrometer (Ettlingen, Germany), using a liquid N_2-cooled MCT detector. Before acquisition of the spectra, the system was purged with nitrogen for at least 30 min. As background, the spectrum of the Ge-ATR crystal in air was used.

Coating stability assessment The stability of the prepared surface coatings was tested in salt water, which was prepared from inorganic salts resembling the major compounds of sea water (31) with ion mass content of >50 ppm, but being free of organic components to avoid the formation of organic deposits on the coatings. The samples were immersed in salt water on a linear shaking table (50 rpm) over 14 d and subsequently rinsed with water and blown dry in a stream of N_2. After this immersion phase, the thickness of the coatings was again determined by spectroscopic ellipsometry, and IR spectra were measured to detect potential changes in the surface chemistry.

Nonspecific adsorption of proteins Non-specific protein adsorption assays were carried out on silicon wafers coated with PFPE-DMA with different chain lengths. Octadecyltrichlorosilane (OTS) coated silicon wafers were used as negative controls. The protocol to assess protein resistance followed earlier publications.(32) In brief, proteins were dissolved in phosphate-buffered saline (PBS, 0.01 M, pH 7.4) at concentrations of 2 $mg \cdot ml^{-1}$ for lysozyme, fibrinogen, and BSA (Table 1). The surfaces were first immersed in 10 mL of PBS for 20 min to allow the coatings to equilibrate before adding 10 ml of protein solution. After 30 min of incubation, samples were gently rinsed with water and dried in a stream of N_2. The thickness of the adsorbed protein adlayer was determined by spectroscopic ellipsometry.

Table 1: Proteins used for the nonspecific adsorption assay, molecular weight, net charge at pH 7.4, and concentration of the proteins in the buffer.

Protein	Molecular weight [g/mol]	Net charge	Protein concentration
Lysozyme	14.7	+	2 mg/ml
Fibrinogen	340	-	2 mg/ml
Albumin (BSA)	66	-	2 mg/ml

Microfluidic diatom accumulation assay Diatom culture and the microfluidic accumulation assay followed previously published protocols.(33) The diatom *Navicula perminuta* was used as a model organism. For the assay, the culture medium was exchanged for filtered seawater (ASW pH 8), and a total cell concentration of 3 million/ml was adjusted using the optical density (OD) at 444 nm. The microfluidic experiment was performed on coated Nexterion B glass slides with OTS as the nonresistant control. IBIDI sticky slides 0.1 (IBIDI, Germany) were glued onto the samples and formed the channel system. For each coating, three accumulation assays were conducted at a constant wall shear stress of 0.22 Pa over 90 min.

To remove any unattached diatoms, pure ASW was rinsed through the channels for 10 min at the same flow speed as used for the accumulation assay. Thirty fields of view (each 0.55 mm²; 830 µm × 665 µm) in the middle of the channel were recorded with an inverted video microscope (Nikon Ti-E, Nikon Japan; 10x phase contrast objective Nikon CFI Plan Fluor DLL NA 0.3, Nikon Japan). To account for slight variations in the physiological state of the diatoms, OTS was included as nonresistant control and the data obtained were normalized to the attachment on OTS. The results presented are the average of three independent assays, error bars represent the standard error (SE). A one-way ANOVA analysis with a post-hoc Tukey test (α=0.05) was used to test if observed differences were statistically significant.

Settlement of zoospores of the green alga *Ulva linza* The settlement of spores of *U. linza* on to the test surfaces followed standard procedures.(34) In brief, spore-bearing fronds of *U. linza* were collected from Craster, Northumberland UK (55°26' N; -1°35' W). Spores were released from the fronds and diluted to produce a suspension containing approx. $1.0x10^6$ ml^{-1} in artificial seawater (ASW) (Tropic Marin). Three replicate coated slides of each test sample were placed in the wells of Quadriperm dishes and 10 ml of the suspension of spores added to each one. The dishes were incubated in the dark for 45 min to allow the spores to attach. Following this the slides were washed in ASW to remove unattached spores before fixing in 2.5% glutaraldehyde in seawater. The densities of spores on the surfaces were counted using a Zeiss Axioscop epifluorescence microscope with image analysis software that detected the fluorescence from the chlorophyll within the spores. The significance of differences between the samples was tested using one-way analysis of variance with a Tukey test (α=0.05). Error bars represent the standard error.

Dynamic short-term field test The dynamic short-term field test was carried out at the biofouling test site at Port Canaveral (28 °24'29.4''N 80°37'37.7''W, Florida, USA) of the Florida Institute of Technology (FIT) using a previously described rotating disk setup.(35) Using a constant rotation speed of 12 rpm, the surfaces were challenged under water at a depth of 0.6 m for 5 days. For fixation, the samples were lifted out of the water and placed for 15 min in a glass compartment containing 0.5 % glutaraldehyde solution in seawater. Afterwards the samples were washed three times with distilled water for 3 min each. Subsequently, the samples were air dried and analyzed by fluorescence microscopy (Nikon Eclipse TE2000-U, 10x phase contrast objective Nikon CFI Plan Fluor DLL NA 0.3, Nikon, Tokyo, Japan) using the autofluorescence of the attached marine organisms. Each chemistry was tested with three replicates and the assay was repeated two times. The diatoms present on the surface were manually counted using the ImageJ 1.5lj software package. A one-way ANOVA analysis with a post-hoc Tukey test (α=0.05) was used to test if observed differences were statistically significant.

3. Results

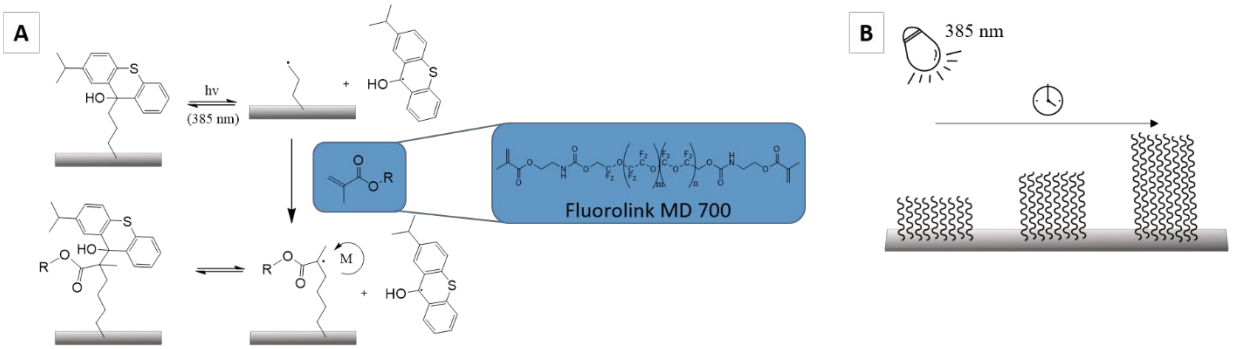

Figure 1: A: Reaction scheme of the visible-light induced surface grafting polymerization on OTS using ITX as the initiator and any methacrylate (RMA) as the monomer. The photoinitiator ITXSP, is reversibly cleaved by visible light (385 nm) releasing a stable ketyl radical (semipinacol) and a free surface radical, allowing the addition of monomers to the surface until recombination with the ketyl radical. B: Schematic illustration of the chain growth of PFPE-DMA over time using visible light (385 nm).

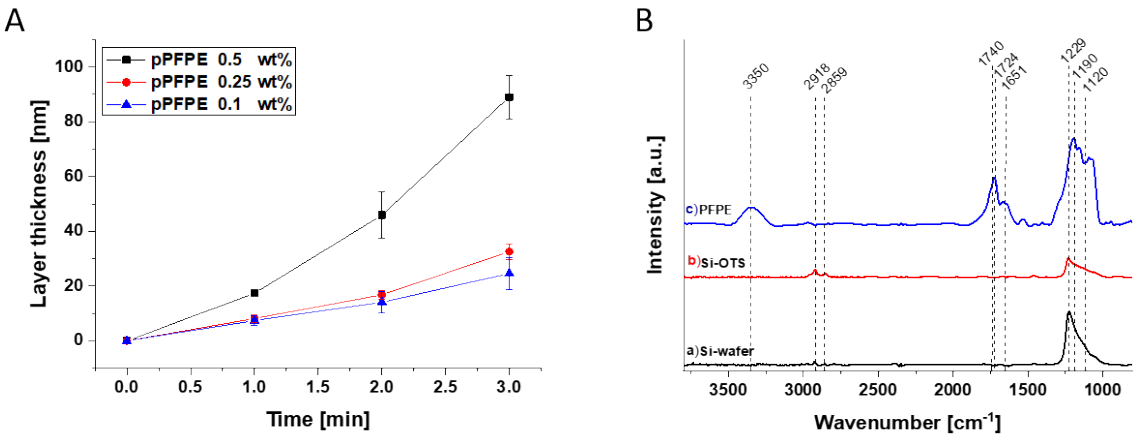

Figure 2: Photoinduced polymerization of PFPE at different monomer concentrations. (A) Thickness of the grafted film as determined by spectroscopic ellipsometry (n=3). Error bars show the standard deviation; (B) ATR-FTIR spectrum of a) unmodified Si-wafer; b) Si-OTS and c) PFPE.

The synthesis of PFPE-DMA brushes (pPFPE) on the surface included several synthesis steps. First, an OTS monolayer was assembled on a substrate (plasma activated silicon and glass) in solution. Secondly, dormant ITXSP groups were introduced by UV light (254 nm) to the surface. Lastly, the surface-bound ITXSP was photoactivated by visible light, producing a radical, which enabled the grafting-from polymerization of PFPE-DMA. The prepared OTS controls were characterized by spectroscopic ellipsometry and contact angle goniometry. Average film thicknesses of 2.6 ± 0.1 nm and CAs of 110° ± 3° were determined and verified the successful film formation.(30) Coupling of the dormant ITXSP groups was characterized by spectroscopic ellipsometry, UV/Vis spectroscopy, IR spectroscopy and contact angle goniometry. Thickness increases of 0.7 ± 0.2 nm were detected as well as absorption bands around 380-420 nm, characteristic for the hydroxyl deformation vibrations δ(OH), while C-H stretch vibrations from the aromatic system became visible at 3000 cm^{-1}. Also, the changed contact angle of 76 ± 3 ° verified the successful coupling of the ITX to the OTS monolayer.

The dormant ITXSP groups that were produced were used as initiating group for the visible light (385 nm) induced polymerization of PFPE-DMA. As the used monomers were dimethacrylates, both ends of

the monomer are in principle capable of being polymerized. Figure 2A shows the increase in layer thickness for three PFPE-DMA concentrations with increasing irradiation time. With increasing monomer concentration, a faster polymerization rate was observed. At the highest PFPE-DMA concentration of 0.5 wt%, the fastest polymerization rate of 26.7 nm/min was detected. The lowest rate was observed at 0.1 wt%, which was about 9.1 nm/min. As shown in Table 2, the water contact angle increased as expected after the growth of the pPFPE brushes which reached 124° ± 9° for the highest layer thickness. This is in good agreement with literature where the contact angle of crosslinked PFPE-DMA coatings has been reported to be 110°± 1°. (21) In order to obtain a deeper insight into the chemistry of the polymerized pPFPE on the organic monolayer OTS and to confirm if the polymerization was successful, ATR-FTIR spectroscopy was applied. The IR spectrum in Figure 2B of the clean silicon substrate shows, as expected, only the Si peak around 1229 cm^{-1}. The OTS-coated surfaces, Figure 2B (b), exhibit the typical aliphatic signals of the SAM layer (30) with the symmetric and antisymmetric CH stretching vibrations at (υ_s CH_2) 2918 cm^{-1} and (υ_{as} CH_2) 2859 cm^{-1}. The IR spectra of PFPE-DMA (pPFPE), Figure 2B (c), show a peak at about 1190 cm^{-1} which can be assigned to the C-F- stretching vibration and a peak at about 1120 cm^{-1} that belongs to the CF-O-CF fluorinated ether group. The peak around 1740 cm^{-1} can be assigned to the carbonyl structures, such as aldehydes or esters, underlining the successful polymerization of PFPE-DMA. The signal at 3350 cm^{-1} is caused by the amine group that is present in the PFPE monomer. With increasing thickness of the PFPE overlayer, the aliphatic signals from the initial silane SAM with the symmetric and antisymmetric CH stretching vibrations at (υ_s CH_2) 2918 cm^{-1} and (υ_{as} CH_2) 2859 cm^{-1} decrease.

Table 2: Static water contact angles of the different coatings for different PFPE-DMA concentrations and different illumination durations. The standard deviation (n = 3) is given as the error.

	OTS	ITX	0.1 PFPE wt%			0.5 PFPE wt%		
Illumination duration /min			1	2	3	1	2	3
Contact angle /°	110 ± 3	76 ± 3	97 ± 5	96 ± 6	104.4 ± 5	97 ± 5	108 ± 4	124 ± 9

Stability of the PFPE-DMA coatings

All coatings for stability assessment and biological tests were prepared using a PFPE-DMA concentration of 0.5 wt%. The thickness was adjusted via the illumination duration (Figure 2a) and is indicated by the number x in the abbreviated sample code pPFPE_x. For the stability tests, 5 nm thick (pPFPE_5), 15 nm thick (pPFPE_15) and 50 nm thick (pPFPE_50) coatings were tested. The stability tests were carried out in salt water (SW) for up to 14 days (Figure 3). The thickness change for all three coatings varied by <10% over the course of the 2 weeks, indicating a high stability.

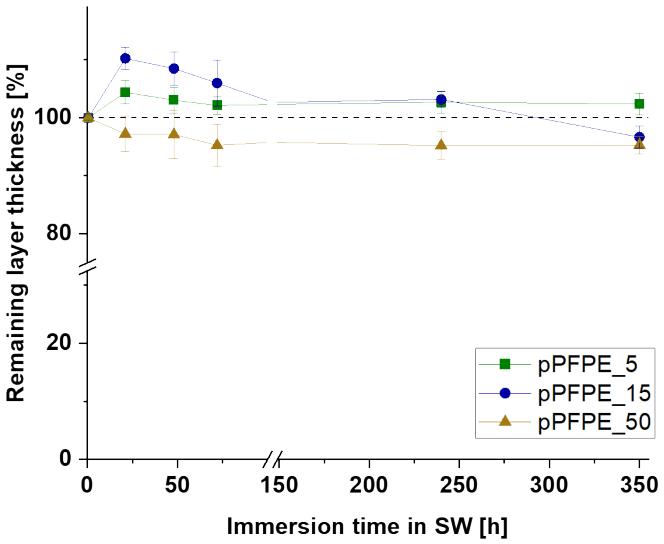

Figure 3: Stability of PFPE-DMA at different chain length in ASW for 14 days (n=3). Error bars represent the standard deviation.

Protein affinity of the PFPE brushes

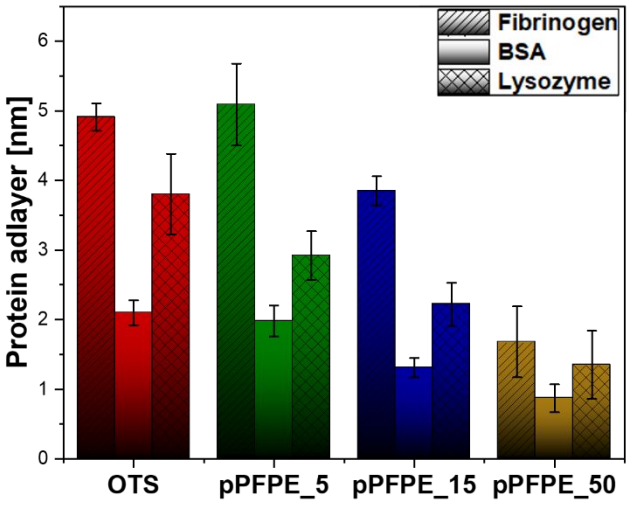

Figure 4: Nonspecific adsorption of proteins on PFPE-DMA coatings with different chain length (n=3). Adlayer thicknesses were determined by spectroscopic ellipsometry (n=3). Error bars represent the standard deviation.

The surfaces were tested against the nonspecific adsorption of different proteins, with varying size and net charge at a pH of 7.4 (see Table 1). The same polymer brush thicknesses as for the stability tests were selected. Figure 4 shows the adlayer thickness after 30 minutes incubation of the OTS controls and three different layer thicknesses of pPFPE in solutions of the proteins fibrinogen, lysozyme, and BSA. The non-specific adsorption of the three proteins on the hydrophobic OTS controls was very similar as on hydrophobic aliphatic SAMs which we previously used as negative controls at the same assay conditions. (36,37) While the 5 nm PFPE-DMA coatings showed only a negligible reduction in attachment of the two

negatively charged proteins BSA and fibrinogen compared to the OTS controls, a greater reduction occurred with the positively charged protein lysozyme. The 15 nm and 50 nm thick PFPE-DMA brushes showed a reduced non-specific protein adsorption for all three proteins compared to OTS. The highest reduction in protein adsorption compared to OTS was found on the 50 nm PFPE-DMA coatings. Here, the nonspecific adsorption of fibrinogen was reduced to 34 %, to 41.4 % for BSA and to 35.5 % for lysozyme compared to the OTS controls.

Dynamic diatom accumulation assay

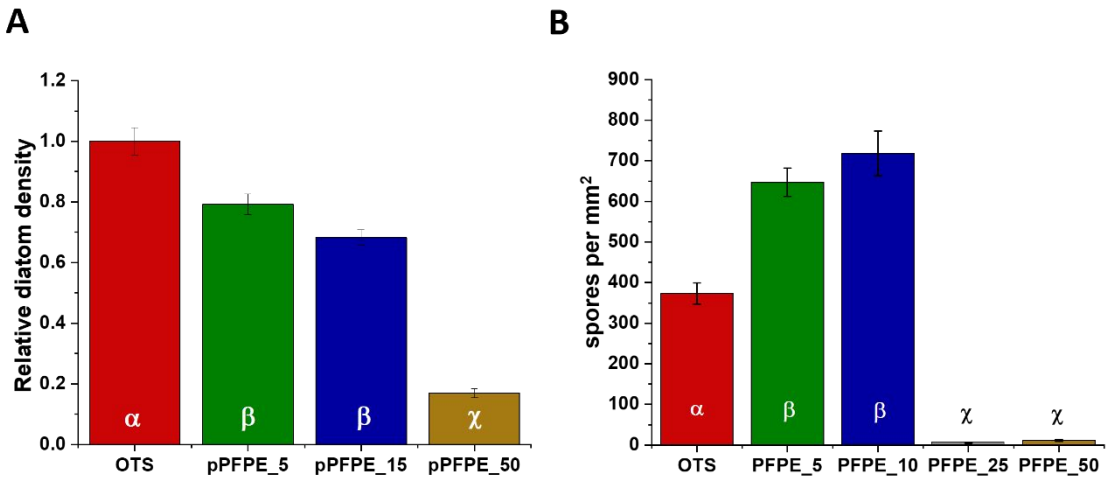

Figure 5: A) Dynamic diatom (Navicula perminuta) accumulation assay with different PFPE-DMA coating thicknesses. The values represent the average of three independent replicates. The error bars represent the standard error of the mean. Bars labelled with different symbols show statistically significant differences ($p<0.05$). Average diatom count on OTS: 159 ± 7 per mm^2. B) Settlement of zoospores of the green algae Ulva linza on PFPE-DMA coatings of different thickness. The values represent the average of three replicate-coated slides. The error bars represent the standard error. Bars labelled with different symbols show statistically significant differences ($p<0.05$).

A microfluidic diatom attachment test was used to probe the initial attachment of diatoms to the coatings. For all surfaces, a significant reduction in diatom accumulation was observed as compared to the nonresistant OTS controls (Figure 5A). Here, the 50 nm thick coatings showed the strongest reduction by 83% in diatom attachment compared to the OTS controls, while 15 nm and 5 nm showed 32 % and 21 % less diatom density compared to the controls, respectively. An ANOVA with post-hoc Tukey test ($p = 0.05$) showed that all observed differences were significant, except between the 5 nm and the 15 nm thick coatings.

Settlement of zoospores of the green algae *Ulva linza*

Spores of the green algae *U. linza* are able to explore and select surfaces suitable for settlement.(38,39) Figure 5B shows the density of zoospores on the PFPE-DMA coatings after the 45 min settlement assay. pPFPE_25 and pPFPE_50 showed a strong and statistically significant reduction by 98% and 97%, respectively, compared to the OTS control. The coatings pPFPE_5 and pPFPE_10 showed higher spore settlement compared to the OTS surface. Here, an increase in settlement by 73% and 92 % was observed. An ANOVA with post-hoc Tukey test ($F_{4, 295} = 112.4$ $P<0.05$) showed that settlement levels on the pPFPE coatings divided into two groups. The first was the pPFPE_5 and pPFPE_10 and the second one, which settlement densities were extremely low, was the pPFPE_25 and pPFPE_50. Settlement on the OTS reference coating was intermediate between the two groups.

Short term dynamic field immersion tests

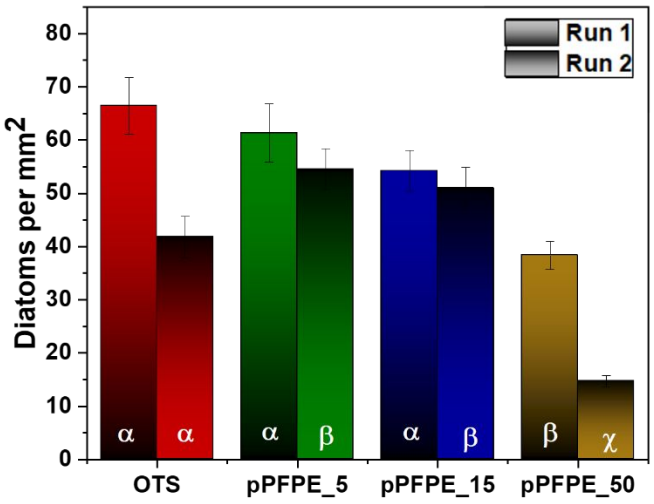

Figure 6: Dynamic short-term field immersion of the different PFPE and OTS coatings. The samples were exposed to the ocean on a rotating disk at a rotation speed of 12 rpm at the FIT test site at Port Canaveral, FL for 5 days. The presented values represent the average of three independent replicates with at least 70 fields of view per slide. Two runs with 3 slides each are shown. The error bars are the standard error of the mean. Significant differences are indicated by different symbols.

Short-term dynamic field immersion tests were carried out to challenge the surfaces against real conditions with a natural mixed species population (Figure 6). Therefore, the surfaces were incubated for 5 days at Port Canaveral, Florida. Two sets of samples were immersed on subsequent weeks. The difference between the two runs could be caused by subtle shifts in the population of fouling organisms due to different currents and nutrient conditions and by difference in weather conditions. The first run showed a lower organism adhesion for the coatings pPFPE_5, pPFPE_25 and pPFPE_50 compared to the OTS coatings. However, a significant reduction was only observed for the pPFPE_50 coatings compared to the negative control OTS. In this case, it was possible to reduce the density of attached species by 42 %. The second run only showed significantly lower adhesion for the pPFPE_50 coatings compared to OTS, but an unusually low attachment to the OTS coatings was noted.

4. Discussion

Using the recently developed ITX mediated grafting-from method(30), perfluoropolyetherdimethacrylate coatings were grown by light-controlled polymerization on silicon and glass surfaces. In a first step, OTS was assembled onto the surfaces causing an increase in contact angle to 110°, with thicknesses of 2.6 nm, which are typical values for silane SAMs. (30) ITXSP was subsequently attached to the monolayers by UV initiation and the successful coupling was confirmed using ATR-FTIR spectroscopy. The contact angle reduced to 76 ± 3 ° and there was an increase in thickness of 0.7 ± 0.2 nm, again in good agreement with previous reports. (30) Lastly, the monomer PFPE was polymerized onto the surface from solution

using a visible light LED source (385 nm). A corresponding increase in layer thickness was observed with increasing polymerization time as well as a faster growth rate with increasing monomer concentration in solution. The fastest growth was observed for the 0.5 wt% solution, exhibiting a rate of 26.7 nm/min. After 5 minutes, an adlayer thickness of 89 nm could be obtained. The successful growth was revealed by the IR modes in the range 1200-1320 cm^{-1}, which are characteristic for C-F vibrational modes and by the signal around 3450 cm^{-1}, which belongs to the N-H valence vibration of the polyurethane groups. All coating thicknesses showed a very high stability in salt water, which was a prerequisite for the bioassays. The prepared coatings were tested against the nonspecific adsorption of different proteins, in single species marine biofouling assays (*N. perminuta, U. linza*), and against a natural mixed fouling organism population in dynamic short-term field exposures. In the protein assays, fibrinogen, lysozyme and BSA showed a decrease in nonspecific adsorption with increasing PFPE film thickness. The reduction was lowest for pPFPE_5, showing a slight reduction in adhesion of the negatively charged fibrinogen and BSA and a minor decrease in adhesion of the positively charged lysozyme. The pPFPE_50 coatings with an even higher contact angle of ~110°, and thus similar contact angles as OTS, showed a reduction in non-specific adsorption for all proteins. Here, the highest reduction of 66 % compared to the OTS control surfaces was observed for fibrinogen. Similar results were obtained for the dynamic accumulation assay using the diatom *N. perminuta* and a reduction of 21 % in diatom attachment was found for the pPFPE_5 coatings compared to the OTS coatings. The pPFPE_50 coatings reduced the adhesion by 83 %. Also, the settlement of *Ulva linza* zoospores showed decreased attachment density on the longer brush lengths. While the coating pPFPE_5 and pPFPE_15 showed a higher attachment compared to OTS, the coatings pPFPE_25 and pPFPE_50 reduced the accumulation by 98 % and 97 %, respectively. In the field tests a significant reduction was only found for the pPFPE_50 coatings. There was a 27 % reduction in the first experiment and 56 % in the second immersion experiment. Thus, despite the relatively high contact angle, the pPFPE_50 coating was surprisingly efficient in reducing the attachment of marine fouling organisms.

Hydrophobic surfaces are in general considered attractive for the nonspecific adsorption of proteins as interactions between van-der Waals forces and the hydrophobic domains of the proteins leads to a strong binding and eventually a denaturation on the surfaces. (40–42) Several studies have also reported the tendency of hydrophobic surfaces to be well colonized by algae and by biofilm-forming microbes. (43,44) Also, diatoms such as *N. perminuta* tend to attach strongly to hydrophobic surfaces. (33,45) PFPE seems to be a material for which not only the surface energy, but also the specific chemistry seems to favor the reduction of fouling. These specific properties have been demonstrated before. For example Yarbrough *et al.* (14) showed reduced settlement of spores of *U. linza* and higher fouling-release properties on cross-linked perfluoropolyether-based graft terpolymers compared to a PDMS elastomer. Our result showed that a grafting-to polymerized, linear PFPE coating had enhanced fouling-release activity that was proportional to increasing coating thickness. The increasing chain length led only to subtle changes of the contact angles, which did not seem to be relevant for the observed attachment of

microbes.

As the wettabilities off all coatings were in a similar range, the detected increase in inertness with increasing polymer brush length was somewhat surprising. One key property that might have been changed by increasing the chain length is the lubricating properties, i.e. the slipperiness of the coating. In previous work it has been reported that the friction coefficient for an $HS(CH_2)_nCH_3$ SAM decreases with increasing chain length. (46) A decrease from 0.52 ± 0.03 for the $C_8H_{17}SH$ SAM to 0.18 ± 0.05 for the $C_{18}H_{37}SH$ SAM, corresponding to a 65.4 % reduction, was reported. (27) Furthermore, Bowen *et al*.(28) reported a significant change in the adhesion of *N. perminuta* and *U. linza* to $HS(CH_2)_nCH_3$ SAMs with different chain lengths. As all surfaces exhibited similar contact angles, it was hypothesized that the lubricity of the surface had a strong influence on the adhesion of the organism. The friction coefficients depend on the packing density, with lower densities leading to lower film thicknesses and consequently to higher friction coefficients. (47) Thus, prior work suggests that better FR performance of thicker monolayers and brushes is related to a reduction of the friction coefficient. In the case of our results, we have to consider that a certain degree of crosslinking between the brushes is likely as a dimethacrylate monomer was chosen. Despite this crosslinking, the coatings obtained seem to be slippery enough to effectively reduce fouling.

5. Conclusion

Within this work we used a controlled polymerization reaction that was visible light-induced to prepare PFPE brushes of different thickness. Therefore, OTS monolayers were assembled onto substrates and a UV-induced coupling of ITX was performed. This surface functionalization was used as the starting point for the controlled growth of PFPE polymers. The coated surfaces were tested for their antifouling properties against diatoms, zoospores, proteins, and challenged in field experiments against the adhesion of a variety of fouling organisms. While the smaller pPFPE coating thicknesses (up to 15 nm) in some cases improved the antifouling capabilities in comparison to the negative reference OTS, the thicker 50 nm pPFPE were a sufficient depth to reduce the attachment of all tested organisms.

6. Conflicts of interest

There are no conflicts of interest to declare

7. Acknowledgements

The work was funded by ONR N00014-16-12979, N00014-20-12244, N00014-20-12248, N00014-13-1-0633, N000141613123 and N000142012243 as well as BMBF 02WIL1487 and the Deutsche Forschungsgemeinschaft (DFG) GRK2376/331085229.

8. References

1. Callow JA, Callow ME. Trends in the development of environmentally friendly fouling-resistant marine coatings. Nat Commun [Internet]. 2011;2(1):210–44. Available from: http://dx.doi.org/10.1038/ncomms1251

2. Rosenhahn A, Schilp S, Kreuzer HJ, Grunze M. The role of “inert” surface chemistry in marine biofouling prevention. Phys Chem Chem Phys [Internet]. 2010;12(17):4275. Available from: http://xlink.rsc.org/?DOI=c001968m

3. Pester CW, Poelma JE, Narupai B, Patel SN, Su GM, Mates TE, et al. Ambiguous anti-fouling surfaces: Facile synthesis by light-mediated radical polymerization. J Polym Sci Part A Polym Chem [Internet]. 2016 Jan 15;54(2):253–62. Available from: https://onlinelibrary.wiley.com/doi/10.1002/pola.27748

4. Paz-Villarraga CA, Castro ÍB, Fillmann G. Biocides in antifouling paint formulations currently registered for use. Environ Sci Pollut Res [Internet]. 2022;29(20):30090–101. Available from: https://doi.org/10.1007/s11356-021-17662-5

5. Wang Y, Betts DE, Finlay JA, Brewer L, Callow ME, Callow JA, et al. Photocurable Amphiphilic Perfluoropolyether/Poly(ethylene glycol) Networks for Fouling-Release Coatings. Macromolecules [Internet]. 2011 Feb 22;44(4):878–85. Available from: https://pubs.acs.org/doi/10.1021/ma102271t

6. Anderson C, Atlar M, Callow M, Candries M, Milne a, Townsin RL. The development of foul-release coatings for seagoing vessels. J Mar Des Oper. 2003;2003(March 2015):11–23.

7. Hu P, Xie Q, Ma C, Zhang G. Silicone-Based Fouling-Release Coatings for Marine Antifouling. Langmuir [Internet]. 2020 Mar 10;36(9):2170–83. Available from: https://pubs.acs.org/doi/10.1021/acs.langmuir.9b03926

8. Nurioglu AG, Esteves ACC, de With G. Non-toxic, non-biocide-release antifouling coatings based on molecular structure design for marine applications. J Mater Chem B [Internet]. 2015;3(32):6547–70. Available from: http://xlink.rsc.org/?DOI=C5TB00232J

9. Camós Noguer A, Latipov R, Madsen FB, Daugaard AE, Hvilsted S, Olsen SM, et al. Visualization of the distribution of surface-active block copolymers in PDMS-based coatings. Prog Org Coatings [Internet]. 2018;120(December 2017):179–89. Available from: https://doi.org/10.1016/j.porgcoat.2018.03.011

10. Callow ME, Fletcher RL. The influence of low surface energy materials on bioadhesion — a review. Int Biodeterior Biodegradation [Internet]. 1994 Jan;34(3–4):333–48. Available from: https://linkinghub.elsevier.com/retrieve/pii/0964830594900922

11. Kroeyer KKK. DT2101074 [Patent]. 1970.

12. Zhang L, Zhou Z, Cheng B, DeSimone JM, Samulski ET. Superhydrophobic Behavior of a Perfluoropolyether Lotus-Leaf-like Topography. Langmuir [Internet]. 2006 Sep 1;22(20):8576–80. Available from: https://pubs.acs.org/doi/10.1021/la061400o

13. Wang Y, Finlay JA, Betts DE, Merkel TJ, Luft JC, Callow ME, et al. Amphiphilic Co-networks with Moisture-Induced Surface Segregation for High-Performance Nonfouling Coatings. Langmuir [Internet]. 2011 Sep 6;27(17):10365–9. Available from: https://pubs.acs.org/doi/10.1021/la202427z

14. Yarbrough JC, Rolland JP, DeSimone JM, Callow ME, Finlay JA, Callow JA. Contact Angle Analysis, Surface Dynamics, and Biofouling Characteristics of Cross-Linkable, Random Perfluoropolyether-Based Graft Terpolymers. Macromolecules [Internet]. 2006 Apr 1;39(7):2521–8. Available from: https://pubs.acs.org/doi/10.1021/ma0524777

15. Williams DN, Shewring, Nigel IE, Lee, Adrian J. Anti-fouling compositions with a fluorinated alkyl- or- alkoxy- containing polymer or oligomer. WO 02/074870 A1 [Patent], 2002.

16. Xiao L, Li J, Mieszkin S, Di Fino A, Clare AS, Callow ME, et al. Slippery liquid-infused porous surfaces showing marine antibiofouling properties. ACS Appl Mater Interfaces. 2013;5(20):10074–80.

17. Epstein AK, Wong T-S, Belisle R a, Boggs EM, Aizenberg J. Liquid-infused structured surfaces with exceptional anti-biofouling performance. Proc Natl Acad Sci U S A [Internet]. 2012 Aug 14 [cited 2013 Aug 10];109(33):13182–7. Available from: http://www.pubmedcentral.nih.gov/articlerender.fcgi?artid=3421179&tool=pmcentrez&rendertype=abstract

18. Wang Z, Heng L, Jiang L. Effect of lubricant viscosity on the self-healing properties and electrically driven sliding of droplets on anisotropic slippery surfaces. J Mater Chem A [Internet]. 2018;6(8):3414–21. Available from: http://xlink.rsc.org/?DOI=C7TA10439A

19. Liu G, Yuan Y, Liao R, Wang L, Gao X. Fabrication of a Porous Slippery Icephobic Surface and Effect of Lubricant Viscosity on Anti-Icing Properties and Durability. Coatings [Internet]. 2020 Sep 18;10(9):896. Available from: https://www.mdpi.com/2079-6412/10/9/896

20. Fang Z, Cheng Y, Yang Q, Lu Y, Zhang C, Li M, et al. Design of Metal-Based Slippery Liquid-Infused Porous Surfaces (SLIPSs) with Effective Liquid Repellency Achieved with a Femtosecond Laser. Micromachines. 2022;13(8).

21. Molena E, Credi C, De Marco C, Levi M, Turri S, Simeone G. Protein antifouling and fouling-release in perfluoropolyether surfaces. Appl Surf Sci [Internet]. 2014 Aug;309:160–7. Available from: http://dx.doi.org/10.1016/j.apsusc.2014.04.211

22. Yao X, Dunn SS, Kim P, Duffy M, Alvarenga J, Aizenberg J. Fluorogel Elastomers with Tunable Transparency, Elasticity, Shape-Memory, and Antifouling Properties. Angew Chemie Int Ed [Internet]. 2014 Apr 22;53(17):4418–22. Available from: https://onlinelibrary.wiley.com/doi/10.1002/anie.201310385

23. Hu Z, Finlay JA, Chen L, Betts DE, Hillmyer MA, Callow ME, et al. Photochemically Cross-Linked Perfluoropolyether-Based Elastomers: Synthesis, Physical Characterization, and Biofouling Evaluation. Macromolecules [Internet]. 2009 Sep 22;42(18):6999–7007. Available from: https://pubs.acs.org/doi/10.1021/ma901227k

24. Matsumoto A, Shimizu K, Mizuta K, Otsu T. Radical polymerization of alkyl crotonates as 1,2-disubstituted ethylenes leading to thermally stable substituted polymethylene. J Polym Sci Part A Polym Chem [Internet]. 1994 Jul 30;32(10):1957–68. Available from: https://onlinelibrary.wiley.com/doi/10.1002/pola.1994.080321019

25. Georges MK, Veregin RPN, Kazmaier PM, Hamer GK, Saban M. Narrow Polydispersity Polystyrene by a Free-Radical Polymerization Process-Rate Enhancement. Macromolecules [Internet]. 1994 Nov 1;27(24):7228–9. Available from: https://pubs.acs.org/doi/abs/10.1021/ma00102a039

26. Yang W, Rånby B. Radical Living Graft Polymerization on the Surface of Polymeric Materials. Macromolecules [Internet]. 1996 Jan 1;29(9):3308–10. Available from: https://pubs.acs.org/doi/10.1021/ma9515543

27. Leggett GJ. Friction force microscopy of self-assembled monolayers: probing molecular organisation at the nanometre scale. Anal Chim Acta [Internet]. 2003 Mar;479(1):17–38. Available from: https://linkinghub.elsevier.com/retrieve/pii/S0003267002015751

28. Bowen J, Pettitt M., Kendall K, Leggett G., Preece J., Callow M., et al. The influence of surface lubricity on the adhesion of Navicula perminuta and Ulva linza to alkanethiol self-assembled monolayers. J R Soc Interface [Internet]. 2007 Jun 22;4(14):473–7. Available from: https://royalsocietypublishing.org/doi/10.1098/rsif.2006.0191

29. Shon Y-S, Lee S, Colorado R, Perry SS, Lee TR. Spiroalkanedithiol-Based SAMs Reveal Unique Insight into the Wettabilities and Frictional Properties of Organic Thin Films. J Am Chem Soc [Internet]. 2000 Aug 1;122(31):7556–63. Available from: https://pubs.acs.org/doi/10.1021/ja000403z

30. Balasubramaniam A, Manderfeld E, Krause LMK, Wanka R, Schwarze J, Beyer CD, et al. Visible light-induced controlled surface grafting polymerization of hydroxyethyl methacrylate from isopropylthioxanthone semipinacol-terminated organic monolayers. Polym Chem [Internet]. 2021;12(4):618–28. Available from: http://xlink.rsc.org/?DOI=D0PY01410A

31. KESTER DR, DUEDALL IW, CONNORS DN, PYTKOWICZ RM. PREPARATION OF ARTIFICIAL SEAWATER1. Limnol Oceanogr [Internet]. 1967 Apr;12(1):176–9. Available from: http://doi.wiley.com/10.4319/lo.1967.12.1.0176

32. Gnanasampanthan T, Beyer CD, Yu W, Karthäuser JF, Wanka R, Spöllmann S, et al. Effect of Multilayer Termination on Nonspecific Protein Adsorption and Antifouling Activity of Alginate-Based Layer-by-Layer Coatings. Langmuir [Internet]. 2021 May 18;37(19):5950–63. Available from: https://pubs.acs.org/doi/10.1021/acs.langmuir.1c00491

33. Nolte KA, Schwarze J, Rosenhahn A. Microfluidic accumulation assay probes attachment of biofilm forming diatom cells. Biofouling [Internet]. 2017 Aug 9;33(7):531–43. Available from: https://doi.org/10.1080/08927014.2017.1328058

34. Cooper SP, Finlay JA, Cone G, Callow ME, Callow JA, Brennan AB. Engineered antifouling microtopographies: kinetic analysis of the attachment of zoospores of the green alga Ulva to silicone elastomers. Biofouling [Internet]. 2011 Sep;27(8):881–92. Available from: http://www.tandfonline.com/doi/abs/10.1080/08927014.2011.611305

35. Nolte KA, Koc J, Barros JM, Hunsucker K, Schultz MP, Swain GW, et al. Dynamic field testing of coating chemistry candidates by a rotating disk system. Biofouling [Internet]. 2018 Apr 21;34(4):398–409. Available from: http://doi.org/10.1080/08927014.2018.1459578

36. Bauer S, Alles M, Arpa-Sancet MP, Ralston E, Swain GW, Aldred N, et al. Resistance of Amphiphilic Polysaccharides against Marine Fouling Organisms. Biomacromolecules [Internet]. 2016 Mar 14;17(3):897–904. Available from: https://pubs.acs.org/doi/10.1021/acs.biomac.5b01590

37. Beyer CD, Reback ML, Heinen N, Thavalingam S, Rosenhahn A, Metzler-Nolte N. Low Fouling Peptides with an All (D) Amino Acid Sequence Provide Enhanced Stability against Proteolytic Degradation While Maintaining Low Antifouling Properties. Langmuir [Internet]. 2020 Sep 22;36(37):10996–1004. Available from: https://pubs.acs.org/doi/10.1021/acs.langmuir.0c01790

38. Heydt M, Pettitt ME, Cao X, Callow ME, Callow JA, Grunze M, et al. Settlement Behavior of Zoospores of Ulva linza During Surface Selection Studied by Digital Holographic Microscopy. Biointerphases [Internet]. 2012 Dec;7(1):33. Available from: http://avs.scitation.org/doi/10.1007/s13758-012-0033-y

39. Callow ME, Callow JA, Pickett-Heaps JD, Wetherbee R. Primary adhesion of Enteromorpha (Chlorophyta, Ulvales) propagules: Quantitative settlement studies and video microscopy. J Phycol. 1997;

40. Prime KL, Whitesides GM. Adsorption of proteins onto surfaces containing end-attached oligo(ethylene oxide): a model system using self-assembled monolayers. J Am Chem Soc [Internet]. 1993 Nov 1;115(23):10714–21. Available from: https://pubs.acs.org/doi/abs/10.1021/ja00076a032

41. Prime KL, Whitesides GM. Self-Assembled Organic Monolayers: Model Systems for Studying Adsorption of Proteins at Surfaces. Science (80-) [Internet]. 1991 May 24;252(5009):1164–7. Available from: https://www.science.org/doi/10.1126/science.252.5009.1164

42. Lu DR, Park K. Effect of surface hydrophobicity on the conformational changes of adsorbed fibrinogen. J Colloid Interface Sci [Internet]. 1991 Jun;144(1):271–81. Available from: https://linkinghub.elsevier.com/retrieve/pii/002197979190258A

43. Maggs CA, Callow ME. Algal Spores. In: eLS [Internet]. Wiley; 2003. p. 1–6. Available from:

http://doi.wiley.com/10.1038/npg.els.0000311

44. Donlan RM. Biofilms: Microbial Life on Surfaces. Emerg Infect Dis [Internet]. 2002 Sep;8(9):881–90. Available from: http://wwwnc.cdc.gov/eid/article/8/9/02-0063_article.htm

45. Alles M, Rosenhahn A. Microfluidic detachment assay to probe the adhesion strength of diatoms. Biofouling [Internet]. 2015;31(5):469–80. Available from: http://dx.doi.org/10.1080/08927014.2015.1061655

46. Brewer NJ, Beake BD, Leggett GJ. Friction Force Microscopy of Self-Assembled Monolayers: Influence of Adsorbate Alkyl Chain Length, Terminal Group Chemistry, and Scan Velocity. Langmuir [Internet]. 2001 Mar 1;17(6):1970–4. Available from: https://pubs.acs.org/doi/10.1021/la001568o

47. Lee S, Shon Y-S, Colorado R, Guenard RL, Lee TR, Perry SS. The Influence of Packing Densities and Surface Order on the Frictional Properties of Alkanethiol Self-Assembled Monolayers (SAMs) on Gold: A Comparison of SAMs Derived from Normal and Spiroalkanedithiols. Langmuir [Internet]. 2000 Mar 1;16(5):2220–4. Available from: https://pubs.acs.org/doi/10.1021/la9909345